Science Bulletin 64 (2019) 888–895

Contents lists available at ScienceDirect

Science Bulletin

journal homepage: www.elsevier.com/locate/scib

Article

Floquet-engineered quantum state transfer in spin chains

Hui Zhou [a], Xi Chen [b,c], Xinfang Nie [d], Ji Bian [b,c], Yunlan Ji [b,c], Zhaokai Li [b,c,e], Xinhua Peng [b,c,e,*]

[a] Department of Physics, Shaanxi University of Science and Technology, Xi'an 710021, China
[b] Hefei National Laboratory for Physical Sciences at the Microscale and Department of Modern Physics, University of Science and Technology of China, Hefei 230026, China
[c] CAS Key Laboratory of Microscale Magnetic Resonance, University of Science and Technology of China, Hefei 230026, China
[d] Department of Physics and Shenzhen Institute for Quantum Science and Engineering, Southern University of Science and Technology, Shenzhen 518055, China
[e] Synergetic Innovation Center of Quantum Information and Quantum Physics, University of Science and Technology of China, Hefei 230026, China

ARTICLE INFO

Article history:
Received 23 April 2019
Received in revised form 20 May 2019
Accepted 20 May 2019
Available online 25 May 2019

Keyword:
Adiabatic quantum optimization
Quantum control
Quantum state transfer
Quantum simulation
Nuclear magnetic resonance

ABSTRACT

Quantum state transfer between two distant parties is at the heart of quantum computation and quantum communication. Among the various protocols, the counterdiabatic driving (CD) method, by suppressing the unwanted transitions with an auxiliary Hamiltonian $H_{cd}(t)$, offers a fast and robust strategy to transfer quantum states. However, $H_{cd}(t)$ term often takes a complicated form in higher-dimensional systems and is difficult to realize in experiment. Recently, the Floquet-engineered method was proposed to emulate the dynamics induced by $H_{cd}(t)$ without the need for complex interactions in multi-qubit systems, which can accelerate the adiabatic process through the fast-oscillating control in the original Hamiltonian $H_0(t)$. Here, we apply this method in the Heisenberg spin chains, with only control of the two marginal couplings, to achieve the fast, high-fidelity, and robust quantum state transfer. Then we report an experimental implementation of our scheme using a nuclear magnetic resonance simulator. The experimental results demonstrate the feasibility of this method in complex many-body system and thus provide a new alternative to realize the high-fidelity quantum state manipulation in practice.

1. Introduction

Quantum state transfer (QST) plays a central role in the field of quantum computation and quantum communication [1,2]. In this respect, spin chains have been considered as good candidates due to the native spin–spin interactions and simple encodings [3–11]. However, many schemes depend on precisely engineering individual couplings as well as accurate timing of dynamic evolution, which is sensitive to practical variations, such as environmental noise, time errors, etc. Due to good robustness against weak variations of the system, the adiabatic passage has been one of the mostly used methods [12–17]. Nevertheless, a common shortcoming of this scheme is that a high-fidelity target state is typically achieved at the cost of time, which may lead to a conflict between the time required by the adiabatic theorem and decoherence time.

To speed up the quantum adiabatic process, an emergent field so-called "shortcut to adiabaticity" (STA) [18–21] has been put forward and now has found applications in a wide range of fields (see Refs. [22,23] for a review of this field). Recently, much effort has been devoted to QST with the help of STA methods [24–27]. For example, Ref. [25] theoretically demonstrated that the non-negligible Dzyaloshinskii-Moriya (DM) interactions in quantum dots can be used to eliminate the undesirable quantum transitions and accelerate the quantum state transfer. In Ref. [26] an odd-spin chain was approximately simplified as a three-spin system based on the weak boundary couplings, and then the shortcut-to-adiabaticity passage was successfully constructed for QST. In addition, by inversely designing the shortcut passage with the quantum Zeno dynamics, Ref. [27] also proposed an ingenious protocol to implement fast QST in a quantum spin chain.

As one of the most successful strategies in STA, counterdiabatic driving (CD) or transitionless driving provides a quite simple way to precisely suppress nonadiabatic transitions by supplementing the original Hamiltonian $H_0(t)$ with a CD term $H_{cd}(t)$ [18,19]. But a general problem with this approach is that the CD term typically consists of complex interactions particularly in multi-qubit system [28–33]. To address this issue, Petiziol et al. [34,35] proposed a method to effectively replicate the dynamics of $H_{cd}(t)$ by periodically modulating the parameters in the original Hamiltonian, which can nullify the need for the complicated terms not included in original quantum system. Similar ideas of accelerating adiabatic process were also recently reported based on Floquet-engineering techniques [36,37].

* Corresponding author.
E-mail address: xhpeng@ustc.edu.cn (X. Peng).

https://doi.org/10.1016/j.scib.2019.05.018
2095-9273/

Inspired by these work, here we put forward an accelerating adiabatic protocol to transfer quantum state across a spin-$\frac{1}{2}$ chains by only modulating two marginal couplings, which can significantly reduce the many multi-body interactions and the experimental difficulties compared with the CD method. Then we also carry out an experiment to demonstrate the validity of our scheme in a four-qubit NMR system. This experiment shows that the Floquet-engineering method can provide a powerful platform for high-fidelity quantum state manipulation in quantum multi-body systems.

2. Method

Recently, Petiziol et al. [34] theoretically explored the relation between the structure of Hamiltonian $H_{\rm cd}(t)$ and the original Hamiltonian $H_0(t)$, and then they proved the following theorem:

Theorem. *Let the Hamiltonian of the system be expressible, at all times and for all values of the control functions* $\boldsymbol{u}(t)=\{u_1(t),\ldots,u_M(t)\}$, *as a linear combination* $H(t)=\sum_{k=0}^{M}u_k(t)H_k$ *of time independent control Hamiltonians* $\boldsymbol{H}=\{H_1,\ldots,H_M\}$. *Let* $\mathcal{L}$ *be the Lie algebra generated by the matrices* $-\mathrm{i}\boldsymbol{H}$. *Assuming the* $H_{\rm cd}$ *exists, then* $-\mathrm{i}H_{\rm cd}(t)$ *belongs to* $\mathcal{L}$, *for all times t.*

This theorem shows that the dynamics of the $H_{\rm cd}(t)$ can be well approximated with an effective counterdiabatic (E-CD) term $H_{\rm E}(t)$ by only modulating the parameters in the system Hamiltonian. The basic procedure to construct the E-CD term is summarized as follows [35]:

(*i*) Obtain the exact CD term $H_{\rm cd}(t)$, and express the E-CD term $H_{\rm E}(t)$ with the control functions $\boldsymbol{c}(t)$

$$H_{\rm E}(t)=\sum_{k=1}^{M}c_k(t)H_k, \tag{1}$$

where $\{H_1,\ldots,H_M\}$ denotes a set of time independent control Hamiltonians in the experiment.

(*ii*) Choose the truncated Fourier series as the control functions

$$c_k(t)=\sum_{j=1}^{L}\left[A_{kj}\sin(j\omega t)+B_{kj}\cos(j\omega t)\right]. \tag{2}$$

Here ω, L, and $\{A_{kj},B_{kj}\}$ denote fundamental frequency, truncated term, and amplitudes, respectively.

(*iii*) Divided the evolution time T into N_t periods and in each small evolution time $\tau=T/N_t=2\pi/\omega$. Then, the amplitudes $\{A_{kj},B_{kj}\}$ can be acquired with the Magnus expansion

$$\begin{aligned}&M^{(1)}(t)=-\tfrac{\mathrm{i}}{\hbar}\int_0^t H(t_1)\mathrm{d}t_1,\\&M^{(2)}(t)=\left(\tfrac{-\mathrm{i}}{\hbar}\right)^2\int_0^t\mathrm{d}t_1\int_0^{t_1}\mathrm{d}t_2[H(t_1),H(t_2)],\\&\cdots\cdots\end{aligned} \tag{3}$$

In this process, we demand the first terms of the Magnus expansion generated by $H_{\rm E}(t)$ coincide with those by the exact term $H_{\rm cd}(t)$ up to a desired order. Finally, with interpolation in different periods, we can obtain the smooth control functions $\{A_{kj}(t),B_{kj}(t)\}$.

3. Application

Spin chain model has been widely studied in many physical systems and played an important role in both condensed-matter physics and quantum computation field [3–5,38–41]. As shown in Fig. 1, the system we considered here involves two qubits A and B weakly coupled to a Heisenberg chain and the whole Hamiltonian is given by

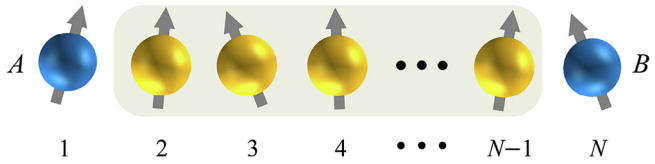

Fig. 1. (Color online) The schematic of QST in the spin chain.

$$H_0(t)=J_A(t)\overrightarrow{\sigma_1}\cdot\overrightarrow{\sigma_2}+J_0\sum_{2}^{N-2}\overrightarrow{\sigma_j}\cdot\overrightarrow{\sigma_{j+1}}+J_B(t)\overrightarrow{\sigma_{N-1}}\cdot\overrightarrow{\sigma_N}, \tag{4}$$

where σ_j are the Pauli matrices for the jth spin, and J_0 is uniform exchange coupling strength in the Heisenberg chain. In this work, we only consider the case $J_0\gg J_A(t),J_B(t)$.

In analogy with other QST protocols, the goal here is to transfer an arbitrary quantum state from qubit A to qubit B, i.e., $|\psi\rangle_A\otimes|0\cdots0\rangle\otimes|0\rangle_B\rightarrow|0\rangle_A\otimes|0\cdots0\rangle\otimes|\psi\rangle_B$, where the quantum state $|\psi\rangle=a|0\rangle+b|1\rangle$ may be in a superposed state defined by $a=\cos\frac{\beta}{2}$, and $b=\mathrm{e}^{\mathrm{i}\alpha}\sin\frac{\beta}{2}$. Notice that $\left[H_0(t),\sum_{n=1}^{N}\sigma_n^z\right]=0$, so the number of excited spins in this process is conserved. In other words, here the QST is restricted within the zero- and one-excitation subspaces. For brevity, we adopted the notaiton as following: the zero-excite state $|\mathbf{0}\rangle=|00\cdots0\rangle$ and the one-excite state $|\mathbf{n}\rangle=\otimes_{m=1}^{N}|\delta_{mn}\rangle$, where $n=1,2,\cdots N$ and δ_{mn} is the Kronecker delta. Thus our QST protocol can be presented as $|\Psi\rangle_i=a|\mathbf{0}\rangle+b|\mathbf{1}\rangle\rightarrow|\Psi\rangle_f=a|\mathbf{0}\rangle+b|\mathbf{N}\rangle$.

On the other hand, due to the strong coupling limit $J_0\gg J_A(t),J_B(t)$ in Eq. (4), the whole system will approximatively evolve in an invariant Zeno subspace consisting of the initial state $|\Psi\rangle_i$ according to quantum Zeno dynamics [42]. As proved by Huang et al. in Ref. [27], here only the Zeno subspace $Z_1=|\mathbf{0}\rangle,|\mathbf{1}\rangle,|\chi\rangle,|\mathbf{N}\rangle$ with the eigenvalue being $(N-3)J_0$ needs considering, and $|\chi\rangle$ is the superposition state of the other one-excited states. Then, the effective Hamiltonian in this Zeno subspace is

$$H_0^{\rm e}(t)=\begin{bmatrix}J_A+J_B & 0 & 0 & 0\\ 0 & -J_A+J_B & \frac{2J_A}{\sqrt{N-2}} & 0\\ 0 & \frac{2J_A}{\sqrt{N-2}} & \frac{(N-4)(J_B+J_A)}{N-2} & \frac{2J_B}{\sqrt{N-2}}\\ 0 & 0 & \frac{2J_B}{\sqrt{N-2}} & J_A-J_B\end{bmatrix}+(N-3)J_0I. \tag{5}$$

Since the last constant term contributes nothing to the dynamical evolution, it can be neglected in the following discussion. Here we set $\hbar=1$, $J_A(t)=J\sin\phi(t)$ and $J_B(t)=J\cos\phi(t)$ with the time-dependent parameter $\phi(t)\in[0,\pi/2]$ and $\frac{J}{J_0}\equiv\alpha\ll1$. Note that the effective Hamiltonian can be always rescaled by an arbitrary factor, and therefore we choose $J=1,\alpha=0.05$ without loss of generality. The eigenvalues of $H_0^{\rm e}(t)$ are $E_{1,2}(t)=\cos\phi(t)+\sin\phi(t)$ and $E_{3,4}(t)=-\frac{\cos\phi(t)+\sin\phi(t)\pm\kappa(t)}{N-2}$ with the time-dependent functions $\eta(t)=(N-1)[\sin\phi(t)-\cos\phi(t)]$ and $\kappa(t)=\sqrt{\eta^2(t)+2\sin2\phi(t)}$. And the corresponding four eigenstates are $|\varphi_1\rangle=[1\quad0\quad0\quad0]^{\rm T}$, $|\varphi_2\rangle=[0\quad1\quad\sqrt{N-2}\quad1]^{\rm T}$, and $|\varphi_{3,4}\rangle=\left[0\quad\frac{\eta(t)\pm\kappa(t)}{2}\quad-\frac{2\cos\phi(t)+\eta(t)\pm\kappa(t)}{2\sqrt{N-2}}\cos\phi(t)\right]^{\rm T}$ apart from the normalized coefficients. Especially at the time $t=0$ and T, the normalized eigenstate $|\varphi_4\rangle$ is

$$|\varphi_4(0)\rangle=\frac{-1}{\sqrt{N^2-N}}\begin{bmatrix}0\\1-N\\\sqrt{N-2}\\1\end{bmatrix},\quad|\varphi_4(T)\rangle=\frac{1}{\sqrt{N^2-N}}\begin{bmatrix}0\\1\\\sqrt{N-2}\\1-N\end{bmatrix}. \tag{6}$$

Thus the initial state $|\Psi\rangle_{\rm i}$ and final state $|\Psi\rangle_{\rm f}$ can be expressed as

$$|\Psi\rangle_{\rm i} = a\,|\varphi_1\rangle + b\frac{1}{\sqrt{N}}|\varphi_2\rangle + b\sqrt{1-\frac{1}{N}}\,|\varphi_4(0)\rangle, \tag{7}$$

$$|\Psi\rangle_{\rm f} = a\,|\varphi_1\rangle + b\frac{1}{\sqrt{N}}|\varphi_2\rangle - b\sqrt{1-\frac{1}{N}}\,|\varphi_4(T)\rangle, \tag{8}$$

which manifest that the high-fidelity QST can be realized as long as the two conditions are satisfied: (*i*) $|\varphi_4(t)\rangle$ are driven adiabatically along its instantaneous eigenstate without any transitions. (*ii*) $|\varphi_4(t)\rangle$ accumulates the additional phase $\vartheta = (2k+1)\pi$ relative to $|\varphi_{1,2}\rangle$ after the time T, here $k \in \mathbb{Z}$. Note that the eigenstates $|\varphi_1\rangle$ and $|\varphi_2\rangle$ are time independent.

Since the minimum gap between $E_3(t)$ and $E_4(t)$ tends to zero with the growth of system size N, the time T guaranteeing the adiabatic condition will increase rapidly. To accelerate the adiabatic process, according to the formula $H_{\rm cd}(t) = {\rm i}\hbar\sum_n |\dot{\varphi}_n(t)\rangle\langle\varphi_n(t)|$ the exact CD term can be calculated:

$$H^{\rm e}_{{\rm cd},N}(t) = {\rm i}f(N,t)\begin{bmatrix} 0 & 0 & 0 & 0 \\ 0 & 0 & 1 & -\sqrt{N-2} \\ 0 & -1 & 0 & 1 \\ 0 & \sqrt{N-2} & -1 & 0 \end{bmatrix}, \tag{9}$$

with the parameter $f(N,t) = -\sqrt{N-2}\dot{\phi}(t)/\kappa^2(t)$. In theory, the adiabatic evolution can be accelerated in a finite duration by directly adding the term $H^{\rm e}_{{\rm cd},N}(t)$ into the original Hamiltonian $H^{\rm e}_0(t)$. However, in many-body systems the CD term always makes trouble as N increases. For example, the term $H^{\rm e}_{{\rm cd},4}(t)$ in this Zeno subspace can be exactly constructed in a four-spins system with ten two-body interactions, twenty three-body interactions and ten four-body interactions. To avoid the tough implementation, we now resort to the Floquet-engineered method.

The Hamiltonian $H^{\rm e}_0(t)$ in Eq. (5) can be rewritten with two control Hamiltonians $H^{\rm e}_1$ and $H^{\rm e}_2$,

$$H^{\rm e}_0(t) = J_A(t)H^{\rm e}_1 + J_B(t)H^{\rm e}_2.$$

Here the two time-independent Hamiltonians read

$$H^{\rm e}_1 = \begin{bmatrix} 1 & 0 & 0 & 0 \\ 0 & -1 & \frac{2}{\sqrt{N-2}} & 0 \\ 0 & \frac{2}{\sqrt{N-2}} & \frac{N-4}{N-2} & 0 \\ 0 & 0 & 0 & 1 \end{bmatrix}, \quad H^{\rm e}_2 = \begin{bmatrix} 1 & 0 & 0 & 0 \\ 0 & 1 & 0 & 0 \\ 0 & 0 & \frac{N-4}{N-2} & \frac{2}{\sqrt{N-2}} \\ 0 & 0 & \frac{2}{\sqrt{N-2}} & -1 \end{bmatrix}, \tag{10}$$

which satisfy the commutation relation $[H^{\rm e}_1, H^{\rm e}_2] = 2{\rm i}H^{\rm e}_3$ and the matrix

$$H^{\rm e}_3 = -{\rm i}\begin{bmatrix} 0 & 0 & 0 & 0 \\ 0 & 0 & \frac{2}{(N-2)^{3/2}} & -\frac{2}{N-2} \\ 0 & -\frac{2}{(N-2)^{3/2}} & 0 & \frac{2}{(N-2)^{3/2}} \\ 0 & \frac{2}{N-2} & -\frac{2}{(N-2)^{3/2}} & 0 \end{bmatrix}. \tag{11}$$

Note the CD term in Eq. (9) can be expressed with $H^{\rm e}_3$, i.e.,

$$H^{\rm e}_{{\rm cd},N}(t) = -\frac{1}{2}f(N,t)(N-2)^{3/2}H^{\rm e}_3 = F_{\rm cd}(t)H^{\rm e}_3. \tag{12}$$

According to the theorem in Section 2, to simulate the dynamic evolution driven by the CD term, the E-CD term can be constructed with the $H^{\rm e}_1$ and $H^{\rm e}_2$,

$$H^{\rm e}_{{\rm E},N}(t) = c_1(t)H^{\rm e}_1 + c_2(t)H^{\rm e}_2. \tag{13}$$

For simplicity, here the control functions $c_{1,2}(t)$ are chosen as

$$c_1(t) = \mathcal{A}\sqrt{\omega}\cos(\omega t), \quad c_2(t) = \mathcal{B}\sqrt{\omega}\sin(\omega t), \tag{14}$$

which can ensure precision of the fidelity at least to first order in τ. During the nth period $[t_n, t_{n+1}]$, the Magnus terms of $H^{\rm e}_{{\rm cd},N}(t)$ and $H^{\rm e}_{{\rm E},N}(t)$ can be computed according to Eq. (9)

$$M_{\rm cd}(\tau) = -{\rm i}\tau F_{\rm cd}(t_n + \tau/2)H^{\rm e}_3 + \mathcal{O}(\tau^3), \tag{15}$$

$$M_{\rm E}(\tau) = -{\rm i}\tau\mathcal{A}\mathcal{B}H^{\rm e}_3 + \mathcal{O}(\tau^{3/2}). \tag{16}$$

To ensure $M_{\rm cd}(\tau) \approx M_{\rm E}(\tau)$ at all the periods, we can get the constraint equations $\mathcal{A}\mathcal{B} = F_{\rm cd}(t)$ for the small τ [34]. Since $F_{\rm cd}(t)$ keeps positive, a simple solution is $\mathcal{A}(t) = \mathcal{B}(t) = \sqrt{F_{\rm cd}(t)}$. So we can obtain the two control functions

$$c_1(t) = \sqrt{F_{\rm cd}(t)\omega}\cos(\omega t), \quad c_2(t) = \sqrt{F_{\rm cd}(t)\omega}\sin(\omega t). \tag{17}$$

Eventually, the complete E-CD Hamiltonian reads

$$H^{\rm e}_{{\rm E},N}(t) = \sqrt{F_{\rm cd}(t)\omega}\left[\cos(\omega t)H^{\rm e}_1 + \sin(\omega t)H^{\rm e}_2\right]. \tag{18}$$

Then, to show the validity of the E-CD term defined above, Fig. 2 reports the numerical simulation results of transferring the eigenstate $|\varphi_4(0)\rangle$ for $N = 4, 8$ with three driving protocols: the native Hamiltonian $H^{\rm e}_0(t)$ (blue dashed lines), the additional CD Hamiltonian $H^{\rm e}_0(t) + H^{\rm e}_{{\rm cd},N}(t)$ (green dashed lines), and the additional E-CD Hamiltonian $H^{\rm e}_0(t) + H^{\rm e}_{{\rm E},N}(t)$ (red solid lines). Here a linear evolution is given by $\phi(t) = \frac{\pi t}{2T}$, and the fidelity is defined by $F(t) = |\left\langle\varphi_4(T)\,|\,\tilde{U}(0,t)\,|\,\varphi_4(0)\right\rangle|^2$ with $\tilde{U}(0,t)$ being the evolution operator produced by the three Hamiltonians from time 0 to t. When the total evolution time $T = 1$, as we can see, the E-CD protocol almost has the same effect of accelerating the adiabatic process with the CD method and the fidelity tends to 1 quickly, which outstrip the native protocol. The slight disparity occurs in the vicinity of the middle part where the nonadiabatic effects are strong. In principle, we can raise the oscillating frequency to acquire higher-precise dynamics simulation by increasing the sampling rates.

Up to now, we have shown the state $|\varphi_4(t)\rangle$ can be driven fast along its instantaneous eigenstate trajectory with the E-CD term, which can greatly reduce the number of many-body interaction terms and the experimental difficulty. However, this will not be enough to transfer an arbitrary quantum state $|\Psi\rangle_i$ to $|\Psi\rangle_f$ due to the possible inaccuracy of the relative phase ϑ at the final time T.

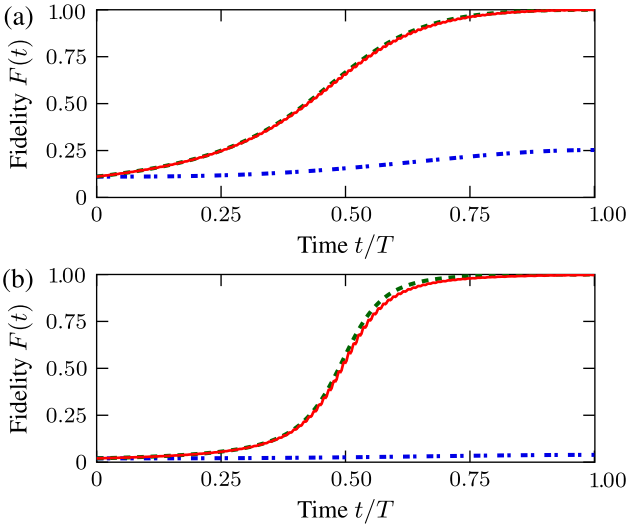

Fig. 2. The fidelity of the state initially evolving from $|\varphi_4(0)\rangle$ for (a) $N = 4$ and (b) $N = 8$ with three protocols: the E-CD method (red line), the exact CD protocol (green dashed line), and naive protocol (blue dashed lines). Here, the parameters are set to be $N_t = 50, T = 1$.

Since the parameter ϑ depends on the time T and the number of periods N_t, it is instructive to look at the fidelity landscapes with the two parameters in specific case and make sure that our scheme works well. For example, Fig. 3 displays the fidelities of transmitting the state $|\psi\rangle = \sin(\pi/3)\,|0\rangle + \cos(\pi/3)\,|1\rangle$ for $N = 4$ and $N = 6$, and both landscapes have some features in common as follows.

Firstly, the high-fidelity area forms the peninsula located on the time T with the increasement of N_t as shown with the purple isolines in Fig. 3. In fact, due to the periodicity of phase, many peninsulas will emerge periodically when we continue to increase time T. The adiabatic path can be tracked as far as possible provided N_t was large enough, but it may lead to higher oscillation frequency ω and stronger couplings according to the Eq. (17), which will hamper the feasibility of experimental implementation. If the limitation of adiabaticity was ruled out at the intermediated times, the fidelity still quickly approaches to 0.99 with relatively low frequency and weak couplings in the added E-CD terms. Furthermore, the fidelity also displays the good robustness against the time T, which can bring much flexibility and agility in experiment.

Secondly, with the periods N_t increasing, the corresponding highest-fidelity time T (red square symbols) approaches to a special time (while line). And here is the reason: In the limit of $N_t \to \infty$, the dynamics of Hamiltonian $H^{e}_{cd,N}(t)$ can be precisely simulated by the $H^{e}_{E,N}(t)$, and the geometric phase $\gamma_n = i\int_0^t dt'\langle\varphi_n(t')\,|\,\partial_{t'}\varphi_n(t')\rangle = 0$. Notice that the eigenvalues $E_1(t) = E_2(t)$, so only the dynamical phase contribute to the relative phase

$$\begin{aligned}\Delta\zeta_N &= \int_0^T [E_{1,2}(t) - E_4(t)]dt \\ &= T\frac{4N - 4 - 4\sqrt{2}\mathbf{E}\left(\frac{\pi}{4}|2N + 1 - N^2\right)}{\pi(N-2)}.\end{aligned} \tag{19}$$

Here $\mathbf{E}(\cdot\,|\,\cdot)$ represents the incomplete elliptic integral of the second kind. When the phase $\Delta\zeta_N$ equals to the target relative phase ϑ, we obtain

$$\Delta\zeta_N = (2k+1)\pi, \quad k \in \mathbb{Z}. \tag{20}$$

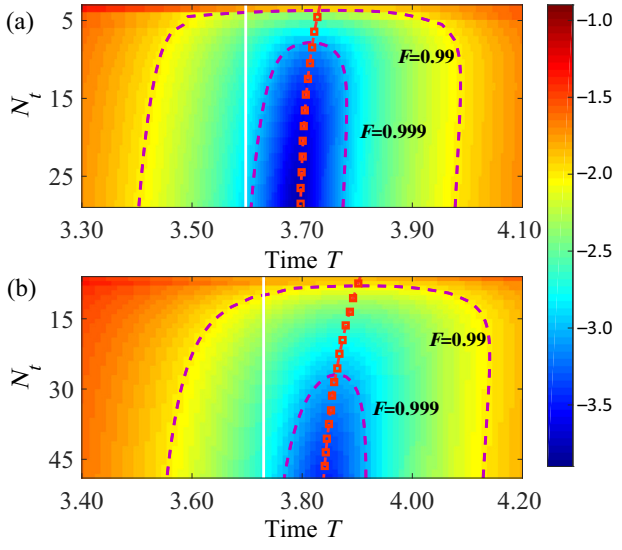

Fig. 3. Infidelity with the different time T and number of the periods N_t for (a) $N = 4$, and (b) $N = 6$. The color bar represents the value of infidelity $F_I(t) = \log_{10}[1 - F(t)]$. The purple dashed isolines denote the fidelity being 0.99 and 0.999, respectively. The red square symbols represent the time of the maximal fidelities for the given N_t, and the white lines denote the time as $N_t \to \infty$. Detailed explanation can be found in the main text.

From the Eqs. (19) and (20), we can obtain the expected time T_s for perfect quantum state transfer with different size N. For example, the time for accumulating π phase are $T_s \approx 3.59,\ 3.75$ for $N = 4, 6$ respectively, which are just displayed as the white lines in Fig. 3a and b. In the limit of $N \to \infty$, the time will converge to the point $T_s \approx 4.21$.

If we use the traditional adiabatic method to transfer the state with the linear sweeping $\phi(t)$, the minimum evolution time for keeping the same final fidelity is $T \approx 11$ for $N = 4$, which shows that the Floquet engineering method can achieve about 3 times speedup. In fact, the speedup will increase with the growth of the system size N, because more times are needed to satisfy the adiabatic theorem compared with our scheme. For example, it will need time $T \approx 19$ to ensure the high-fidelity QST with the traditional adiabatic method for $N = 6$, while the E-CD protocol only need $T \approx 3.8$ to reach the same fidelity.

To investigate the robustness of our scheme in the whole spin systems described by Eq. (4), we add the fast oscillation term to the original Hamiltonian $H_0(t)$ and obtain

$$H(t) = \eta_1(t)\overrightarrow{\sigma_1}\cdot\overrightarrow{\sigma_2} + J_0\sum_2^{N-1}\overrightarrow{\sigma_j}\cdot\overrightarrow{\sigma_{j+1}} + \eta_2(t)\overrightarrow{\sigma_{N-1}}\cdot\overrightarrow{\sigma_N}, \tag{21}$$

where the parameters are $\eta_1(t) = c_1(t) + J_A(t)$ and $\eta_2(t) = c_2(t) + J_B(t)$ with $c_1(t)$ and $c_2(t)$ given by the Eq. (17). Here we focus on the four-spin system and choose the parameters $(T, N_t) = (3.72, 8)$ from the Fig. 3a with the fidelity being about 0.999. The fidelity against the imperfection of amplitudes in the functions $\eta_1(t)$, $\eta_2(t)$ was numerically calculated. As shown in Fig. 4, even if the relative errors $|\delta\eta_1/\eta_1| = 10\%$ and $|\delta\eta_2/\eta_2| = 10\%$, the final fidelity still keeps above 0.97, which manifests that our scheme holds good robustness against the errors in practice. In a larger system, the validity and robustness of this scheme still exist as long as the inner coupling strength $J_0 \gg \eta_1, \eta_2$.

What's more, this method can refrain from using the multibody interactions and speed up the adiabatic process, which will reduce the experimental complexity compared with the CD method. For example, since the inherent multibody interaction is absent in NMR, we have to simulate it with many radio-frequency pulses and two-body interactions. Therefore, errors accumulated from the decoherence effect and imperfect operations will increase the difficulty in experiments. In brief, this method

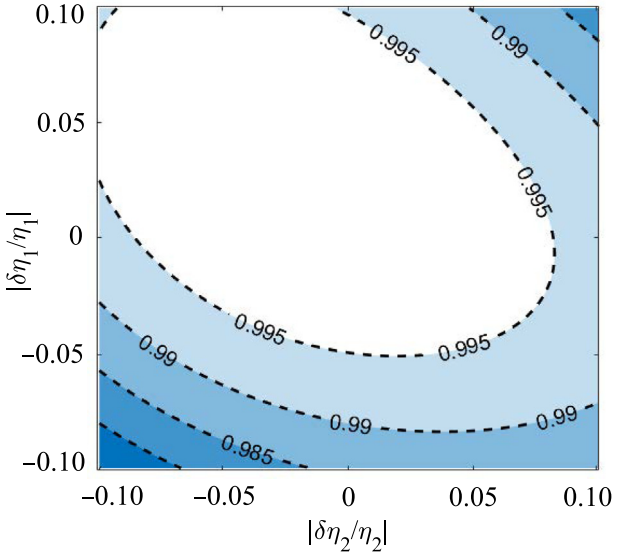

Fig. 4. Quantum state fidelity vs. the imperfection of two amplitudes in control functions $\eta_1(t)$ and $\eta_2(t)$.

provides new control knobs to speed up adiabatic protocols with available resources in experiment, and in the next section we will demonstrate our scheme experimentally with an NMR simulator.

4. Experiments setup and results

The experiment was carried out on a Bruker AV-400 spectrometer (9.4T) at room temperature. The iodotrifluoroethylene dissolved in d-chloroform was used as a four-qubit quantum system to simulate the spin chains. The natural abundance of the sample with a single ^{13}C is about 1%. To distinguish those molecules against the large background, we read out the signals of all three ^{19}F qubits via the ^{13}C channel. The natural Hamiltonian of this system in the double rotating frame is

$$H_{\rm nmr} = \sum_{i=1}^{4} \pi \nu_i \sigma_i^z + \sum_{i<j,=1}^{4} \frac{\pi J_{ij}}{2} \sigma_i^z \sigma_j^z, \tag{22}$$

where ν_i is the chemical shift of spin i and J_{ij} is the scalar coupling constant between spin i and j. The values of these system parameters are shown Fig. 5a. The experiment consists of the following steps.

(*i*) *Initial state preparation*

Starting from the equilibrium state, we first initialized the system into the pseudopure state (PPS) with the line-selective method [43,44]:

$$\rho_{\rm pps} = \frac{1-\varepsilon}{16} I_{16} + \varepsilon |0000\rangle\langle 0000|, \tag{23}$$

where I_{16} represents the 16×16 unity operator and $\varepsilon \approx 10^{-5}$ is the polarization. The NMR spectrum of the PPS after applying a readout pulse to the first qubit is shown in Fig. 5b.

To prepare the initial state, the local pulses $R_x(\frac{\pi}{2}) - R_y(\alpha) - R_x(-\frac{\pi}{2}) - R_y(\beta)$ were applied to first qubit. Here the operator $R_\mu(\theta) = \exp[-i\theta\sigma^\mu/2]$ denotes the single-bit operation along μ direction ($\mu = x, y, z$). We chose the parameters $(\alpha, \beta) = (0, 2\pi/3)$ and $(\pi/3, \pi/4)$ to create two sets of the initial states $|\Psi(0)\rangle = \cos(\pi/3)\,|\mathbf{0}\rangle + \sin(\pi/3)\,|\mathbf{1}\rangle$ and $|\Psi(0)\rangle = \cos(\pi/8)\,|\mathbf{0}\rangle + e^{i\pi/3}\sin(\pi/8)\,|\mathbf{1}\rangle$, respectively. In order to ensure these states successfully prepared, we performed the full state tomography [45,46]. In our experiments, the amplitudes of spectra were obtained by a fit to Lorentzians. Fig. 6f show the

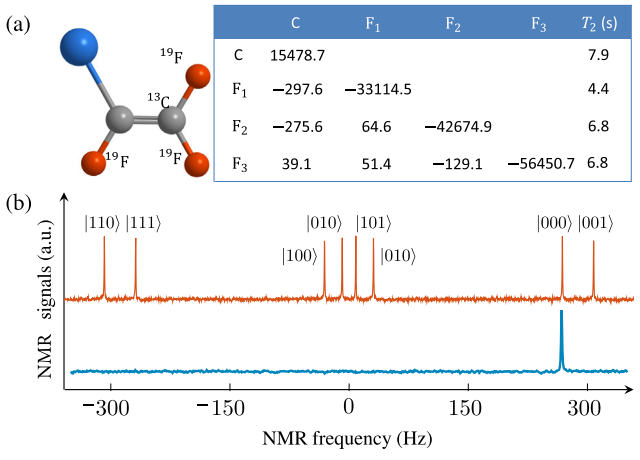

	C	F_1	F_2	F_3	T_2 (s)
C	15478.7				7.9
F_1	−297.6	−33114.5			4.4
F_2	−275.6	64.6	−42674.9		6.8
F_3	39.1	51.4	−129.1	−56450.7	6.8

Fig. 5. (Color online) (a) Molecular structure and relevant parameters of iodotrifluoroethylene at 303 K. The chemical shifts and *J*-coupling constants are on and below the diagonal (in Hz) in the table, respectively. (b) Experimental ^{13}C spectrum of the equilibrium state (orange line) and the pseudopure state (blue line) after a $\pi/2$ readout pulse along y axis. The eight resonance lines are labeled by the corresponding states of the other three qubits.

reconstructed density matrixes for the two states respectively, from which we acquired the state fidelities about 99.3%, and the fidelity is defined by [47]

$$F = \frac{{\rm Tr}\left(\rho_{\rm exp}\rho_{\rm th}\right)}{\sqrt{{\rm Tr}\left(\rho_{\rm exp}^2\right){\rm Tr}\left(\rho_{\rm th}^2\right)}}. \tag{24}$$

Here $\rho_{\rm exp}$ and $\rho_{\rm th}$ represent the experimentally measured density matrix and the ideal expectation. The blue lines in Fig. 6i and j denote the experimental spectra of two initial states, respectively.

(*ii*) *Dynamic evolution along the engineered paths*

The key step in our experiment is to implement the QST with engineered paths $H(t)$ as described in Eq. (21). The evolution operator $U(0,T)$ from time 0 to T is given by

$$U(0,T) = \mathcal{T}\left(e^{-i\int_0^T H(t){\rm d}t}\right),$$

where $\mathcal{T}$ denotes the time-ordering operator. For the experimental implementation, the continuous passage was discretized into M steps [48–50], and in the mth step $H(t)$ can be expressed as

$$H[t_m] = \sum_{\mu=x,y,z}\left(\eta_1[t_m]\cdot\sigma_1^\mu\sigma_2^\mu + \eta_2[t_m]\cdot\sigma_{N-1}^\mu\sigma_N^\mu + J_0\sum_2^{N-1}\sigma_i^\mu\sigma_{i+1}^\mu\right), \tag{25}$$

with the discrete parameters $\eta_1[t_m] = c_1(t_m) + J_A(t_m), \eta_2[t_m] = c_2(t_m) + J_B(t_m), t_m = mT/M = m\Delta t$ and $m = 1, 2, \cdots, M$. The evolution operator in the mth step is $U_m = e^{-i\Delta t H[t_m]}$, and in the limit of $M \to \infty$ and $\Delta t \to 0$ the total time evolution operator is given by

$$U(0,T) = \prod_{m=1}^{M} U_m = \prod_{m=1}^{M} e^{-i\Delta t H[t_m]}, \tag{26}$$

which can be further decomposed into the single-qubit operations and free evolutions with the Trotter expansion [51]. As shown in Fig. 7, direct implementation of this pulse sequence in experiment will accumulate systematic errors and significant decoherence effect. To overcome these problems and reach a high-fidelity quantum coherent control, here the discrete steps was numerically optimized as $M = 100$ and the unitary operator U in Eq. (26) can keep the final states fidelity above 0.996. Then we packed the operator into one shaped pulse calculated by the gradient ascent pulse engineering (GRAPE) method [52–55], with a duration of 25 ms. The shaped pulse is designed to be robust against the inhomogeneity of the practical control field and has numerical fidelities over 0.995.

(*iii*) *Readout and state tomography*

To examine if the target states were sent to the end of spin chains, we performed state tomography on the final states as shown in Fig. 6c,d and g, h. The red lines in Fig. 6i and j denote the experimental spectra after a $\pi/2$ readout pulse applied to first qubit. The final fidelities of the four-bit density matrix are about 98.5%. By tracing over the sending and inner spins, we obtained the reduced density matrixes of the receiving spin $\overline{\rho}_1 = \begin{bmatrix} 0.275 & 0.379 + 0.008i \\ 0.379 - 0.008i & 0.725 \end{bmatrix}$ and $\overline{\rho}_2 = \begin{bmatrix} 0.819 & 0.170 - 0.296i \\ 0.170 + 0.296i & 0.181 \end{bmatrix}$, of which the fidelities are all above 99.5%. These experimental results clearly demonstrate the successful implementation of the high-fdelity QST across the Heisenberg spin chains with the Floquet-engineered method.

The infidelities of the final states in experiment were about 2%, which mainly come from the imperfection of the initial state and GRAPE pulses, and decoherence. Using the experimentally

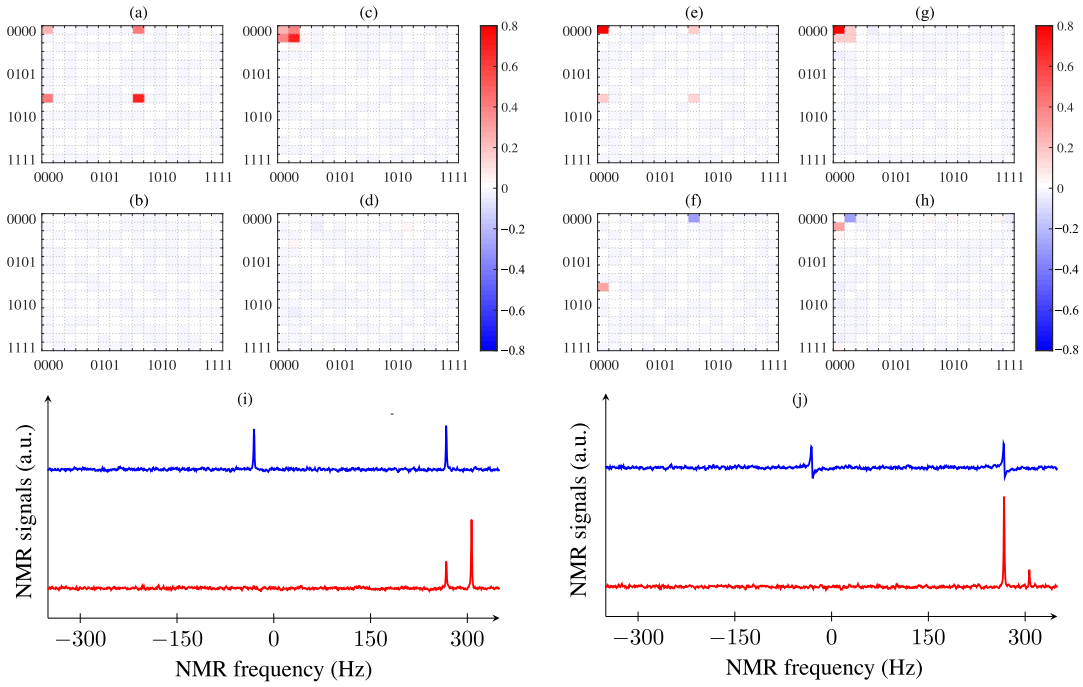

Fig. 6. (a)–(h) Experimental density matrix of the two initial states: (a, b) $|\Psi(0)\rangle = \cos(\pi/3)\,|\mathbf{0}\rangle + \sin(\pi/3)\,|\mathbf{1}\rangle$, (e, f) $|\Psi(0)\rangle = \cos(\pi/8)\,|\mathbf{0}\rangle + e^{i\pi/3}\sin(\pi/8)\,|\mathbf{1}\rangle$ and the corresponding final states (c, d) and (g, h). Here the upper and under figures denote the real and imaginary components, respectively, and the rows and columns in each subfigure represent the standard computational basis in binary order from $|0000\rangle$ to $|1111\rangle$. (i) and (j) denote the ^{13}C signals of the two sets of states as above. The blue spectrum denotes the initial state after a $R_x(\pi/2)$ pulse applied to the third qubit, and red spectrum denotes the final state after a $R_y(\pi/2)$ pulse applied to the first qubit.

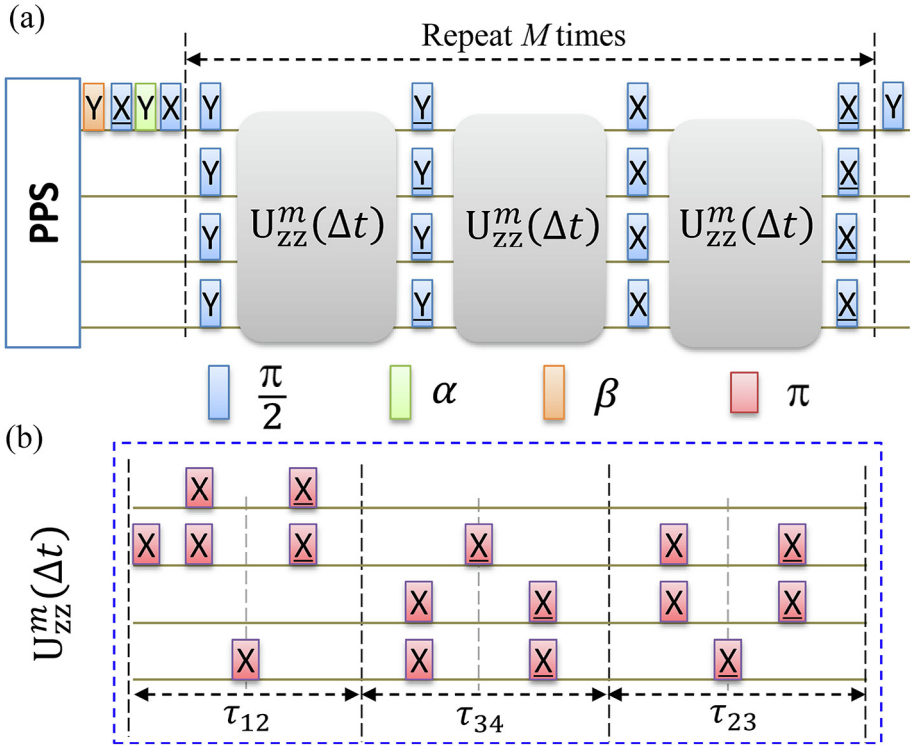

Fig. 7. (a) Pulse sequence for simulating the dynamic evolution with the Trotters formula, and here the gray rectangle denotes the operator $U_{zz}^{m}(\Delta t) = \exp\left[-i\Delta t(\eta_1[t_m]\cdot\sigma_1^z\sigma_2^z + J_0\sigma_2^z\sigma_3^z + \eta_2[t_m]\cdot\sigma_3^z\sigma_4^z)\right]$, which can be realized with the pulse sequence in (b). The other color rectangles represent the hard pulses applied to individual qubits and pulse phases is indicated inside them. Time durations $\tau_{12} = \frac{2\Delta t\cdot\eta_1[t_m]}{\pi|J_{12}|}$, $\tau_{34} = \frac{2\Delta t\cdot\eta_2[t_m]}{\pi|J_{34}|}$, $\tau_{23} = \frac{2\Delta t\cdot J_0}{\pi|J_{23}|}$ represent free evolutions under the natural Hamiltonian.

reconstructed density matrix, we find that the imperfection of initial state contributes about 1% to the errors. Besides, numerical simulations reveal that the GRAPE pulse will produce errors less than 1%. The duration of each experiment is about 25 ms, which is short compared to the relaxation time $T_2^* \approx 1.2$ s, and therefore the effect of decoherence should be relatively small.

5. Conclusion

In summary, based on the Floquet-engineering techniques [34,35], we here put forward a novel accelerating adiabatic protocol for high-fidelity QST in spin chains by approximatively counteract nonadiabatic transitions. This protocol can be implemented by only modulating two marginal couplings, which can significantly reduce the number of many-body interactions and the experimental difficulties compared with the CD method. Furthermore, we experimentally investigate the performance of our protocol in a four-qubit NMR system. This experiment demonstrates the feasibility of this method via current technology, which provides an effective method for high-fidelity quantum state manipulation in complex and noisy quantum systems, and has applications in many areas, such as entanglement creation [50], quantum heat engines [56], and quantum phase transition [28].

Conflict of inerest

The authors declare that they have no conflict of interest.

Acknowledgments

This work was financially supported by the National Natural Science Foundation of China (11847016, 11425523 and 11661161018), National Key Research and Development Program of China (2018YFA0306600), and Anhui Initiative in Quantum Information Technologies (AHY050000).

Author contributions

H. Zhou designed and carried out the experiments; X. Chen, X. Nie, J. Bian and Y. Ji performed the numerical simulations; H. Zhou and Z. Li wrote the paper and all authors discussed the contents; X. Peng supervised the whole project.

References

[1] Nielsen MA, Chuang IL. Quantum computation and quantum information. Cambridge Univ Press; 2000.
[2] Bose S. Quantum communication through spin chain dynamics: an introductory overview. Contemp Phys 2007;48:13.
[3] Bose S. Quantum communication through an unmodulated spin hain. Phys Rev Lett 2003;91:207901.
[4] Friesen M, Biswas A, Hu X, et al. Quantum communication through an unmodulated spin hain. Phys Rev Lett 2007;98:230503.
[5] Paganelli S, Lorenzo S, Apollaro TJG, et al. Routing quantum information in spin chains. Phys Rev A 2013;87:062309.
[6] Wu L-A, Liu Y-X, Nori F. Universal existence of exact quantum state transmissions in interacting media. Phys Rev A 2009;80:042315.
[7] Ashhab S, de Groot PC, Nori F. Speed limits for quantum gates in multiqubit systems. Phys Rev A 2012;85:052327.
[8] Oh S, Shim Y-P, Fei J, et al. Resonant adiabatic passage with three qubits. Phys Rev A 2013;87:022332.
[9] Ashhab S. Quantum state transfer in a disordered one-dimensional lattice. Phys Rev A 2015;92:062305.
[10] Oh S, Wu L-A, Shim Y-P, et al. Heisenberg spin bus as a robust transmission line for quantum-state transfer. Phys Rev A 2011;84:022330.
[11] Qin W, Wang C, Long GL. High-dimensional quantum state transfer through a quantum spin chain. Phys Rev A 2013;87:012339.
[12] Della Valle G, Ornigotti M, Fernandez TT, et al. Adiabatic light transfer via dressed states in optical waveguide arrays. Appl Phys Lett 2008;92:011106.
[13] Jong LM, Greentree AD, Conrad VI, et al. Coherent tunneling adiabatic passage with the alternating coupling scheme. Nanotechnology 2009;20:405402.
[14] Farooq U, Bayat A, Mancini S, et al. Adiabatic many-body state preparation and information transfer in quantum dot arrays. Phys Rev B 2015;91:134303.
[15] Chen B, Peng Y-D, Li Y, et al. Robust multiple-range coherent quantum state transfer. Sci Rep 2016;6:28886.
[16] Petrosyan D, Nikolopoulos GM, Lambropoulos P. State transfer in static and dynamic spin chains with disorder. Phys Rev A 2010;81:042307.
[17] Longhi S. Coherent transfer by adiabatic passage in two-dimensional lattices. Ann Phys 2014;348:161.
[18] Berry MV. Transitionless quantum driving. J Phys A 2009;42:365303.
[19] Demirplak M, Rice SA. Adiabatic population transfer with control fields. J Phys Chem A 2003;107:9937.
[20] del Campo A. Shortcuts to adiabaticity by counterdiabatic driving. Phys Rev Lett 2013;111:100502.
[21] Masuda S, Nakamura K. Fast-forward of adiabatic dynamics in quantum mechanics. Proc R Soc 2010;A466:1135.
[22] Torrontegui E, Ibanez S, Martinez-Garaot S, et al. Shortcuts to adiabaticity. Adv At Mol Opt Phys 2013;62:117.
[23] del Campo A, Kim K, Focus on shortcuts to adiabaticity. arxiv:1902.06283, 2019.
[24] Baksic A, Belyansky R, Ribeiro H, et al. Shortcuts to adiabaticity in the presence of a continuum: applications to itinerant quantum state transfer. Phys Rev A 2017;96:021801(R).
[25] Shi X, Yuan H, Mao X, et al. Robust quantum state transfer inspired by Dzyaloshinskii-Moriya interactions. Phys Rev A 2017;95:052332.
[26] Agundez RR, Hill CD, Hollenberg LCL, et al. Superadiabatic quantum state transfer in spin chains. Phys Rev A 2017;95:012317.
[27] Huang B-H, Kang Y-H, Chen Y-H, et al. Quantum state transfer in spin chains via shortcuts to adiabaticity. Phys Rev A 2018;97:012333.
[28] del Campo A, Rams MM, Zurek WH. Assisted finite-rate adiabatic passage across a quantum critical point: exact solution for the quantum Ising model. Phys Rev Lett 2012;109:115703.
[29] Ibáñez S, Chen X, Torrontegui E, et al. Multiple Schrödinger pictures and dynamics in shortcuts to adiabaticity. Phys Rev Lett 2012;109:100403.
[30] Takahashi K. Transitionless quantum driving for spin systems. Phys Rev E 2013;87:062117.
[31] Sels D, Polkovnikov A. Minimizing irreversible losses in quantum systems by local counterdiabatic driving. Proc Natl Acad Sci USA 2017;114:E3909.
[32] Baksic A, Ribeiro H, Clerk AA. Speeding up adiabatic quantum state transfer by using dressed states. Phys Rev Lett 2016;116:230503.
[33] Li Y-C, Chen X. Shortcut to adiabatic population transfer in quantum three-level systems: effective two-level problems and feasible counterdiabatic driving. Phys Rev A 2016;94:063411.
[34] Petiziol F, Dive B, Mintert F, et al. Fast adiabatic evolution by oscillating initial Hamiltonians. Phys Rev A 2018;98:043436.
[35] Petiziol F, Dive B, Carretta S, et al. Accelerating adiabatic protocols for entangling two qubits in circuit QED. Phys Rev A 2019;99:042315.
[36] Boyers E, Pandey M, Campbell DK, et al. Floquet-engineered quantum state manipulation in a noisy qubit. arXiv:1811.09762, 2018.
[37] Bukov M, Sels D, Polkovnikov A. Geometric speed limit of accessible many-Body state preparation. Phys Rev X 2019;9:011034.
[38] Peng X, Zhou H, Wei B-B, et al. Experimental observation of Lee-Yang zeros. Phys Rev Lett 2015;114:010601.
[39] Li J, Fan R, Wang H, et al. Measuring out-of-time-order correlators on a nuclear magnetic resonance quantum simulator. Phys Rev X 2017;7:031011.
[40] Zeiher J, Choi J-Y, Rubio-Abadal A, et al. Coherent many-body spin dynamics in a long-range interacting Ising chain. Phys Rev X 2017;7:041063.
[41] Zhang J, Pagano G, Hess PW, et al. Observation of a many-body dynamical phase transition with a 53-qubit quantum simulator. Nature 2017;551:601.
[42] Facchi P, Pascazio S. Quantum Zeno subspaces. Phys Rev Lett 2002;89:080401.
[43] Gershenfeld NA, Chuang IL. Bulk spin-resonance quantum computation. Science 1997;275:350.
[44] Peng X, Zhu X, Fang X, et al. Preparation of pseudo-pure states by line-selective pulses in nuclear magnetic resonance. Chem Phys Lett 2001;340:509.
[45] Lee J-S. The quantum state tomography on an NMR system. Phys Lett A 2002;305:349.
[46] Peng X, Luo Z, Zheng W, et al. Experimental implementation of adiabatic passage between different topological orders. Phys Rev Lett 2014;113:080404.
[47] Teklemariam G, Fortunato EM, Pravia MA, et al. NMR analog of the quantum disentanglement eraser. Phys Rev Lett 2001;86:5845.
[48] Peng X, Wu S, Li J, et al. Observation of the ground-state geometric phase in a Heisenberg XY model. Phys Rev Lett 2010;105:240405.
[49] Li Z, Zhou H, Ju C, et al. Experimental realization of a compressed quantum simulation of a 32-Spin Ising chain. Phys Rev Lett 2014;112:220501.
[50] Ji Y, Bian J, Chen X, et al. Experimental preparation of Greenberger-Horne-Zeilinger states in an Ising spin model by partially suppressing the nonadiabatic transitions. Phys Rev A 2019;99:032323.
[51] Suzuki M. General decomposition theory of ordered exponentials. Proc Jpn Acad Ser 1993;B69:161.
[52] Khaneja N, Reiss T, Kehlet C, et al. Optimal control of coupled spin dynamics: design of NMR pulse sequences by gradient ascent algorithms. J Magn Reson 2005;172:296.
[53] Nie X, Huang J, Li Z, et al. Experimental demonstration of nonlinear quantum metrology with optimal quantum state. Sci Bull 2018;63:469–76.
[54] Li K, Wan Y, Hung L-Y, et al. Experimental identification of non-abelian topological orders on a quantum simulator. Phys Rev Lett 2017;118:080502.
[55] Lu D, Li K, Li J, et al. Enhancing quantum control by bootstrapping a quantum processor of 12 qubits. npj Quantum Inf 2017;3:1038.
[56] del Campo A, Goold J, Paternostro M. More bang for your buck: super-adiabatic quantum engines. Sci Rep 2014;4:6208.

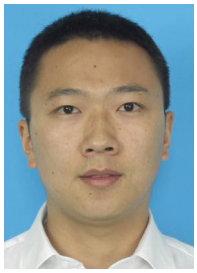

Hui Zhou received his Ph.D. degree from University of Science and Technology of China in 2016. He is now a lecturer of Shaanxi University of Science and Technology. His research interests include quantum computation and quantum simulation.

Xinhua Peng received her Ph.D. degree in atomic and molecular physics in 2003 from the Wuhan Institute of Physics and Mathematics, Chinese Academy of Sciences (Wuhan, China). She is now a professor of University of Science and Technology of China. Her research interests include quantum computation, quantum simulation and quantum control based on NMR, basic problems of quantum mechanics and Low-field nuclear magnetic resonance by atomic magnetometer.